MID-AMERICA TRANSPORTATION CENTER

Report # MATC-UI: 142-3

Final Report
WBS: 25-1121-0005-142-3

Infrastructure Inspection During and After Unexpected Events – Phase III

Salam Rahmatalla, PhD
Professor
Department of Civil and Environmental Engineering
The University of Iowa

Ali Karimpour, MSc
Research Assistant
Department of Civil and Environmental Engineering
The University of Iowa

2021

A Cooperative Research Project sponsored by
U.S. Department of Transportation- Office of the Assistant Secretary for Research and Technology

MATC

Infrastructure Inspection During and After Unexpected Events – Phase III

Salam Rahmatalla, PhD
Professor
Civil and Environmental Engineering
University of Iowa

Ali Karimpour, MSc
Research Assistant
Civil and Environmental Engineering
University of Iowa

A Report on Research Sponsored by

Mid-America Transportation Center

University of Nebraska-Lincoln

November 2021

Technical Report Documentation Page

<table>
<tr><td colspan="2">1. Report No.
25-1121-0005-142-3</td><td>2. Government Accession No.</td><td colspan="2">3. Recipient's Catalog No.</td></tr>
<tr><td colspan="3" rowspan="2">4. Title and Subtitle
Infrastructure Inspection during and after Unexpected Events
Third Year Final Report and Outcomes</td><td colspan="2">5. Report Date
November 2021</td></tr>
<tr><td colspan="2">6. Performing Organization Code</td></tr>
<tr><td colspan="3">7. Author(s)
Salam Rahmatalla, Ali Karimpour</td><td colspan="2">8. Performing Organization Report No.
25-1121-0005-142-3</td></tr>
<tr><td colspan="3" rowspan="2">9. Performing Organization Name and Address
University of Iowa
Department of Civil and Environmental Engineering
4105 Seamans Center for the Engineering Arts and Sciences
Iowa City, Iwa, 52242</td><td colspan="2">10. Work Unit No. (TRAIS)</td></tr>
<tr><td colspan="2">11. Contract or Grant No.
69A3551747107</td></tr>
<tr><td colspan="3" rowspan="2">12. Sponsoring Agency Name and Address
Mid-America Transportation Center
2200 Vine St.
PO Box 830851
Lincoln, NE 68583-0851</td><td colspan="2">13. Type of Report and Period Covered
January 2020 – December 2020</td></tr>
<tr><td colspan="2">14. Sponsoring Agency Code MATC
MATC TRB RiP No. 91994-49</td></tr>
<tr><td colspan="5">15. Supplementary Note</td></tr>
<tr><td colspan="5">16. Abstract
This report presents the development of a new methodology called bridge loading capacity prediction (BLCP). The proposed method also presents a new rating factor (RF) estimation. An updated bridge finite element model (FEM) is deployed to represent a numerical model of a prototype for BLCP application. The methodology iteratively imposes traffic loads on the bridge FEM until the 3D failure criteria is met as the ultimate load-carrying capacity of the bridge. The results obtained by the proposed method were compared with conventional as well as experimental results from a well-documented bridge model. The proposed BLCP can also be appended to commercial RF software and could help the Department of Transportation make quick decisions about issuing permits to trucks that can safely cross the bridge.</td></tr>
<tr><td colspan="3">17. Key Words
Structural Model Validation (SMV), Finite Element Model (FEM), Highway Bridges.</td><td colspan="2">18. Distribution Statement</td></tr>
<tr><td>19. Security Class if. (of this report)
Unclassified</td><td colspan="2">20. Security Class if. (of this page) Unclassified</td><td>21. No. of Pages
29</td><td>22. Price</td></tr>
</table>

Table of Contents

List of Figures

Acknowledgments

The authors would like to thank Dr. Sanayei and his colleagues for publishing comprehensive experimental data from a real bridge model that other scholars can use to validate their numerical methods.

Disclaimer

The contents of this report reflect the views of the authors, who are responsible for the facts and the accuracy of the information presented herein. This document is disseminated under the sponsorship of the U.S. Department of Transportation's University Transportation Centers Program, in the interest of information exchange. The U.S. Government assumes no liability for the contents or use thereof.

Executive Summary

This report presents the development of a new methodology called bridge loading capacity prediction (BLCP). The proposed method also presents a new rating factor (RF) estimation. An updated bridge finite element model (FEM) is deployed to represent a numerical model of a prototype for BLCP application. The methodology iteratively imposes traffic loads on the bridge FEM until the 3D failure criteria are met as the ultimate load carrying capacity of the bridge. The results obtained by the proposed method were compared with conventional as well as experimental results from a well-documented bridge model. The proposed BLCP can also be appended to commercial RF software and could help the Department of Transportation make quick decisions about issuing permits to trucks that can safely cross the bridge.

Chapter 1 Introduction and Background

Highway bridges' load-carrying capacity index provides a comprehensive integrity assessment tool for engineers to use for bridge rating (Lee et al., 2006). The service live load that can be safely carried over a bridge is called the load rating and is expressed as a rating factor (RF). To have a consistent index of load-carrying capacity, all bridges are rated by a standard set of heavy trucks called legal loads (LL). Concurrent highway bridge rating in the USA is commanded by American Association of State Highway Transportation Officials (AASHTO) Load Resistance Factor Design (LRFD) Bridge Design Specifications (AASHTO, 2017). The load and resistance factor rating (LRFR) method provides the RF formula for new and existing bridges as the ratio of specific LL resistance to design LL including its dynamic effects and associated uncertainties. The RF shows the number of a particular truck type or LL that can safely cross the bridge. The LL models are the design live load, legal live load, and permit live load.

The design live load rating is based on a design load (HL-93 truck type) and the LRFD design standard. It is done at a high reliability level (Inventory Level) and a low reliability level (Operating Level). Bridges that attain an RF higher than the Inventory Level are safe for all LL, and there is no need for ratings in further stages. The legal live load rating rates bridges with a truck configuration other than HL-93. A bridge that passes the LL rating can be assessed for a permit load rating. Actions such as load posting, repair, replacement, or closure can be taken when a bridge fails to pass the LL rating. Load posting enforces weight limits on highway bridge traffic and severely attenuates freight mobility (Russian et al., 2020). There are two general types of bridge ratings based on the associated reliability index, inventory rating, and operating rating. The inventory rating aims to reach a high reliability index ($\beta = 3.5$), and the operating rating

aims to reach a lower reliability index ($\beta = 2.5$) by prescribing an appropriate load and resistance coefficient in the RF formula. A bridge rating can be performed at the strength limit state (SLS) and checked for serviceability limits. In addition to analytical load rating, experimental testing often takes place to rate bridges, dictate rehabilitation plans, and compute live load distribution and dynamic impact factors. There are two experimental tests: proof load testing and diagnosis load testing. In proof load testing, a bridge is loaded incrementally until it reaches a target live load to determine model capacity. Diagnosis load testing is performed to validate numerical finite element model (FEM) and physical model responses (Varela-Ortiz et al., 2013).

Most previous studies and concurrent RF evaluation approaches focus on individual components rather than bridge behavior as a whole. The concurrent AASHTO approaches to estimating RF for a real bridge model consist of transforming the bridge superstructure into an equivalent composite T-beam, consequently imposing traffic loading based on girder distribution factors and LL distribution factors. The live load distribution factor is based on linear elastic analysis to apply system overall live load effects on each girder (Dymond et al., 2019). The AASHTO Manual for Bridge Evaluation (MBE) (AASHTO, 2018) provides several formulas to estimate the girder and LL distribution factors for interior and exterior girders; they indicate the percentage of total moment resisted by an individual girder based on empirical, statistical, and simplified equivalent composite section properties. The codified load rating methods return conservative outcomes due to code simplifications, system overall composite action loss, and stirrups elimination when they use beam-line analysis and live load distribution factors (Jamali et al., 2019). Plus, during common bridge load rating, the positive and negative moment regions must be investigated separately due to their different failure mechanisms and the switching of

tension and compression regions in concrete. Although for a single-span or multi-span simply supported bridge there is no negative moment, for a continuous-span bridge the negative moment could be the governing spot during load rating (Tohme & Yarnold, 2020).

The FEM is widely used in bridge engineering for capacity evaluation or to investigate complex incidents such as truck collision with bridge piers (Cao et al., 2019; Xu et al., 2019). The effect of intermediate diaphragms on the load-carrying capacity of a box girder bridge was investigated by nonlinear FEM under concentrated loads at the middle span (Vu et al., 2018). A parametric study to investigate individual structural characteristics on the overall shear capacity and shear distribution factors in elastic ranges was numerically performed and showed that AASHTO factors return conservative results (Dymond et al., 2019). An FEM platform and reliability-based design optimization were proposed to detect critical LL in which the target reliability index is found with the lowest computational cost (Siavashi & Eamon, 2019). A new wavelet-based energy rate index and an updated FEM of a steel truss bridge prototype were exploited for structural health monitoring, damage detection, and load rating (Shahsavari et al., 2020). Recently, a nonlinear FEM of a bridge was used as an efficient approach for RF estimation through the proxy section method (Schanck & Davids, 2020). Prevalent commercial software (e.g., CSI Bridge, AASHTOWare) also convert a bridge FEM into a transformed T-beam reinforced concrete deck and steel girder sections as a function of girder spacing, span length, slab thickness, and distribution factors (Aghagholizadeh & Catbas, 2019; AASHTO, 2020). These FEM packages use almost the same process to estimate RF via computer rather than manual calculation.

This report proposes a new weight-based algorithm, bridge loading capacity prediction (BLCP), to swiftly rate bridge structures with an integrated decision-making protocol based on a

calibrated FEM to return a unique RF of the whole model. Instead of evaluating the capacity demand of moments and shear forces due to LL and using transformed composite T-beams along with AASHTO beam-line analysis, the methodology imposes direct incremental lane loading up to the ultimate bridge capacity where all elements in a segment reach the yielding threshold. The bridge 3D FEM is artificially segmented into several segments, each of which may contain various elements and materials. Suitable failure criteria based on individual element material type are deployed to detect bridge capacity for the sake of a unique RF estimation. Using BLCP, the Department of Transportation (DOT) may express an overall structural system RF with a unique RF for further legal action in limiting traffic volume.

Chapter 2 Bridge Load Rating Methods

The next two sections describe the conventional AASHTO RF method and the proposed RF estimation approach.

2.1 AASHTO Rating Factor (RF) method

Three AASHTO design philosophies—allowable stress rating (ASR), load factor rating (LFR), and LRFR—have been developed over decades. The comprehensive approach to quantifying a highway bridge's capability to bear a service traffic load is described by the MBE (AASHTO, 2018) as follows:

$$RF = \frac{C-(\gamma_{DC})(DC)-(\gamma_{DW})(DW)\pm(\gamma_P)(P)}{(\gamma_{LL})LL(1+IM)} \quad (2.1)$$

where C is capacity, DC is dead load effect, DW is wearing surface effect, P is permanent load, LL is live load, and IM is dynamic load allowance. For an inventory level with a high reliability index ($\beta = 3.5$), the LL coefficient is $\gamma_{LL} = 1.75$, and for an operating level with a lower reliability index ($\beta = 2.5$), $\gamma_{LL} = 1.35$. The dead load factor is $\gamma_{DC} = 1.25$, and the wearing surface load factor is $\gamma_{DW} = 1.50$ for the SLS. The capacity C for SLS can be estimated as:

$$C = \varphi_c \varphi_s \varphi R_n \quad (2.2)$$

$$\varphi_c \varphi_s \geq 0.85 \quad (2.3)$$

where φ_c, φ_s, φ, and R_n are the condition factor, system factor, resistance factor, and nominal member resistance specified by LRFD code, respectively (AASHTO, 2017). The condition factor φ_c provides a reduction in strength due to the uncertainty in member resistance ranging from

0.85 to 1.00. The system factor φ_s and LRFD resistance factor φ are specified by code based on their limit states. For service limit states, the capacity C is:

$$C = f_R \tag{2.4}$$

where f_R is allowable stress specified by LRFD code. The RF obtained by the previous formula can be exploited to find the safe load capacity (RT) of the bridge in tonnage:

$$RT = RF \times W \tag{2.5}$$

where W is the truck net weight used during RF estimation as the LL. Though the strength is the primary limit state for load rating, service and fatigue limit states must be applied for practical applications

2.2 BLCP method

This section introduces the BLCP methodology as shown in Figure 2.1. Through this weight-based process, there is no need to use empirical formulas, live load distribution factors, or the transformed simplified T-beam approach; however, all safety factors in capacity and demand prescribed by Equation (2.1) are incorporated in BLCP.

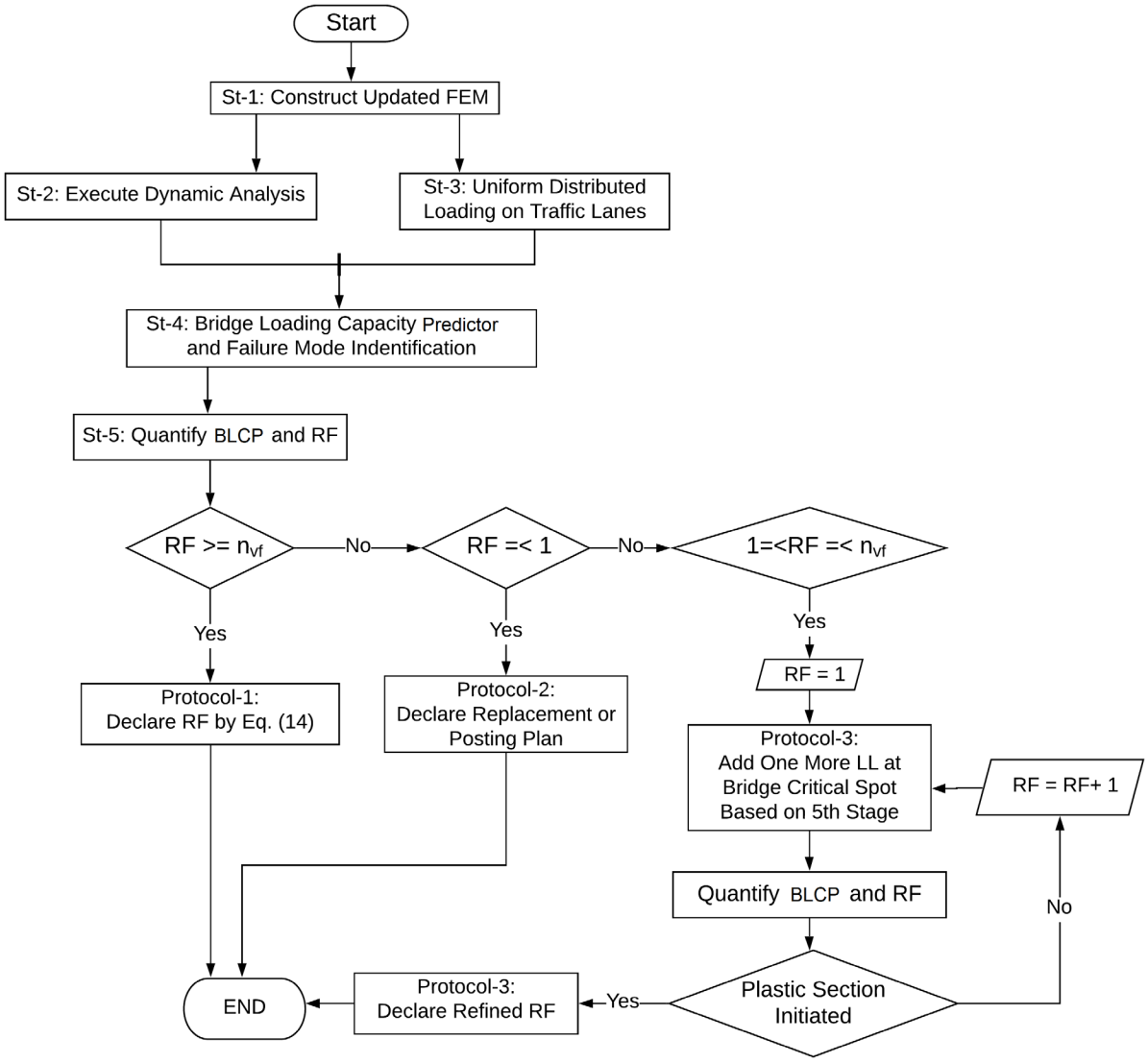

Figure 2.1 Flow chart of the proposed weight-over process (BLCP).

A unique RF, rather than several values, is required to decide how many trucks can pass over a bridge model simultaneously. Also, the potential failure mode under excessive traffic loading and potential critical load configurations/positions could illuminate infrastructure flaws for rehabilitation purposes.

2.2.1 Stage (1): Construct updated (calibrated) FEM

The first step is to construct an accurate FEM of the bridge and calibrate it from its in situ data (Shahsavari et al., 2020). Various model-updating procedures are available by which FEM would be a genuine representative of the physical model. The most important parameter that affects a bridge structure's capacity is material property, and it must be accurately estimated for further FEM analysis (Russian et al., 2020). Nonlinear material models must be incorporated to develop BLCP so it can capture yielding of the bridge in the plastic region. Thus, all material and geometric nonlinearities effects plus the large displacement effects must be activated to make the FEM an authentic representative of its prototype.

2.2.2 Stage (2): Dynamic load allowance and impact factor (IM)

The coupled vehicle-bridge interaction problem is one of the most interesting numerical and theoretical simulation issues studied by scholars for decades (Tian & Zhang, 2020). There are various approaches, ranging from simple assumptions of moving loads to the more precise moving vehicle body, for simulating and solving vehicle-bridge interaction (Benčat & Kohár, 2018). To evaluate dynamic induced effects on a bridge model, the LRFD dynamic load allowance or IM can be estimated from the FEM with the following equation:

$$IM = \frac{S_{dyn} - S_{sta}}{S_{sta}} \tag{2.6}$$

where S_{dyn} is the peak value of the dynamic structural response and S_{sta} is the static structural response caused by the same action(s) or under the same load combination situation, estimated based on the most crucial of the understudied bridge points. AASHTO prescribed using HL-93 design truck loading for IM estimation only. The AASHTO formula for IM is (AASHTO, 2017):

$$IM = 0.33(1.0 - 0.125D_E) \geq 0 \quad (2.7)$$

where D_E is the minimum depth of earth cover above the structure (ft). Practically, the IM value is estimated from the bridge surface condition: 11% for fine, smooth asphalt; 22% for intermediate clearness; and 33% at most for a very bad surface. AASHTO suggests using $IM = 0.33$ in order to attain high reliability when no in situ experimental testing or numerical modeling is performed. While some reported that IM values might be much higher than the AASHTO-prescribed ones, up to $IM = 2.80$, it depends on the bridge type, structural geometry, road surface condition, and truck speed (Deng et al., 2011). Numerical studies showed that road surface condition is the major factor in prescribing the IM during bridge loading capacity evaluation (Deng & Cai, 2010). Since the bridge's structural system and its characteristics could have strong effects on IM value, it is recommended to quantify IM through a numerical dynamic analysis for any understudied bridge.

2.2.3 Stage (3): Uniform distributed load (UDL) on traffic lanes

Pushover analysis is a robust tool in structural seismic analysis that aims to evaluate ultimate structure capacity, model performance, and potential failure modes under lateral loading imposed by earthquakes (Liu et al., 2020; Peng et al., 2020). By mimicking the pushover analysis concept from seismic engineering, the BLCP offers an analogous approach to truly evaluate the loading capacity, with several suitable modifications. The realistic vehicular loading is composed of several pressure areas dictated by type of vehicle and axle configuration. The UDL theory says equivalent UDLs produce the same secondary effects on structural components as a set of discrete loads (Bakht & Mufti, 2015). Therefore, the UDL pattern on the traffic lanes at the tire lines are imposed on the FEM nodes to represent the tire effective lines during BLCP analysis.

For instance, consider an HL-93 truck, which is defined by AASHTO as the design LL for a bridge, composed of three axles with a total LL weight of $W_{LL} = 325(KN)$, an overall vehicle length of $L_{LL} = 8.6(m)$, and left-side tires spaced $L_{lr} = 1.8(m)$ from the right-side tires. In this step, regardless of the LL truck weight itself, only the tire contact patch area (250 mm X 510 mm) and the rear distance are used to select affected FEM nodes, supposing that each truck passes exactly in the center of each traffic lane. After assigning N_{nl} FEM nodes for each traffic lane, each FEM node is uniformly loaded and its load-displacement curvature as well as stress, strain, and deflection are supervised until the stop criteria are met. Each FEM nodal load F_m during BLCP is recorded and will be summed to estimate the ultimate bearable weight in the form of UDL. In other words, all N_{nl} of FEM nodes at all N_{tl} traffic lanes are statically loaded until yield criteria are met. The dynamic effects can be adjusted in the RF formula from the guidelines described in the previous stage. It must be noted that, based on Equation (2.1), the factored dead load $\gamma_{DC}(DC)$, factored wearing surface load $\gamma_{DW}(DW)$, and factored permanent load $\gamma_P(P)$ must be defined in FEM as an active load combination before imposing BLCP loading to be consistent with the AASHTO formula.

2.2.4 Stage (4): BLCP and failure mode identification

To perform BLCP analysis, the whole bridge FEM is equally segmented across its length (Z-direction in current FEM) to as many segments as its mesh size length "M_s". At each segment, there are "N_m" number of element sets; that "N_m" is equal to the number of materials of which the bridge model is made. By now, the FEM is partitioned into the "$M_s * N_m$" number of element sets along the bridge model while each element set attains identical material type. To track the location of different segments on the bridge, each segment resides inside a station. BLCP will have information about the location of each station across the bridge. All elements at each station

attain the same pivotal coordinate along the bridge span length. While the bridge span is loaded through BLCP, some elements at several sets start to pass their yield thresholds; however, the LRFD criteria dictate that the whole section yields. The first section at a station in which all elements pass their yield stress is called the plastic section (PS).

Since just the authentic traffic paths are loaded through BLCP, the genuine failure mode can be detected consequently. In general, shear failure mode and flexural failure mode are the dominant modes for steel plate girder bridges (Alinia et al., 2009). Failure modes of bridge spans are mostly shear-induced, flexural-induced, and combined shear-flexural-induced modes. Shear mode failure happens very close to the beginning and end stations, while flexural failure happens in the middle of the bridge. Many studies have shown that shear-induced failure at girders is much more dangerous than flexural failure due to its abrupt collapse nature; this must be prohibited by appropriate design guidelines (Dymond et al., 2019). Even though shear-induced, moment-induced, and combined shear-moment-induced plastic hinges can be considered for 1D structural members, BLCP brought the PS concept for 3D FEM during RF estimation. For single-span bridges or multi-span simply supported bridges, the initiation of the first PS starts the collapse phenomenon due to instability and shows the ultimate load. For continuous multi-span bridges, the BLCP UDL can be further increased after the first PS initiation due to structural redundancy at their boundary conditions (Deng & Phares, 2016).

At each FEM segment residing at a specific station defined by BLCP, there are several element sets, each consisting of few materials. Since each material yields different thresholds and criteria for each set of elements, the appropriate failure criteria must be applied to estimate PS genesis. Since BLCP deals with the 3D FEM of a composite bridge prototype with various materials, appropriate failure criteria must be chosen to reconcile and compare the 3D FEM

stress field to the uniaxial stress-strain curve of each material. Thus, BLCP automatically computes all components' interaction actions (axial-shear-flexural) and compares appropriate equivalent stress to material yield stress. The Von Mises yield criteria is used to capture 3D yielding of FEM elements of steel components. For flexible components made with metallic materials, the Von Mises stress or equivalent stress (σ_e) is commonly used as the failure criteria (Rosendahl et al., 2019):

$$\sigma_e = \sqrt{\frac{1}{2}((\sigma_1 - \sigma_2)^2 + (\sigma_1 - \sigma_3)^2 + (\sigma_3 - \sigma_2)^2)} = \sigma_y \tag{2.8}$$

where σ_1, σ_2, σ_3, and σ_y are the first, second, and third principal stresses and the uniaxial yield stress, respectively, while $\sigma_1 \geq \sigma_2 \geq \sigma_3$. For structural parts made with brittle materials such as concrete, the maximum principal stress (σ_{mps}) is normally used as the failure criteria. The maximum principal criteria states that yield occurs when the largest principal stress exceeds its correspondent uniaxial yield strength (Leckie & Bello, 2009); it is expressed as:

$$\sigma_{mps} = \begin{cases} \sigma_1 \geq \sigma_{yc} \\ OR \\ |\sigma_3| \geq |\sigma_{yt}| \end{cases} \tag{2.9}$$

where σ_{yc} and σ_{yt} are compressive strength and tensile strength, respectively. It must be noted that any other failure criteria could be deployed to execute BLCP based on material types and engineering judgment. The force-displacement curve is commonly used by structural engineers to detect yielding and the ultimate capacity of structures, as well as to visualize structural

response trends before and after yielding (Garcia et al., 2019). The BLCP can be calculated from its FEM whenever the first segment(s) see all element sets pass the associated yielding criteria. This means that the ultimate model capacity is when, at specific FEM station(s), all concrete element sets pass σ_{mps} and all steel element sets pass σ_e as defined in Equations (2.8) and (2.9), respectively. At this point, the first PS is initiated, the total section is yielded, and system stability depends on available structural redundancy. Now, the critical weight (W_{cr}) of an understudied bridge can be computed by BLCP from its FEM by summing all nodal force (F_m) of all predefined traffic lanes:

$$W_{cr} = \sum_{n=1}^{N_{tl}} \left[\sum_{m=1}^{N_{nl}} F_m \right] \tag{2.10}$$

where N_{tl} and N_{nl} are the number of traffic lanes and the number of FEM nodes for each traffic lane for the specific bridge model. It must be noted that since the factored dead load, wearing surface, and permanent load were inserted in the previous stage on the FEM before implementing BLCP, this critical weight (W_{cr}) is equivalent to the unfactored nominal resistance of the FEM; all effects other than LL were considered as follows:

$$W_{cr} = \frac{C - (\gamma_{DC})(DC) - (\gamma_{DW})(DW) \pm (\gamma_P)(P)}{\varphi_c \varphi_s \varphi} \tag{2.11}$$

Equation (2.11) expresses the unfactored system leftover capacity estimated by BLCP after considering other effects in terms of structural system weight. Therefore, the numerator of the RF formula in Equation (2.1) can be estimated from the following formula:

$$[C - (\gamma_{DC})(DC) - (\gamma_{DW})(DW) \pm (\gamma_P)(P)] = (\varphi_c \varphi_s \varphi) * W_{cr} \tag{2.12}$$

2.2.5 Stage (5): Quantify BLCP and declare its RF

The critical weight (W_{cr}) at which a bridge collapses under excessive traffic loading was calculated in the previous stage with the UDL concept, and the potential bridge failure mode was perceived by investigating the PS as described in the BLCP stage. Three possibilities can occur based on two quantities. The first quantity is the bridge characteristic value (n_{vf}), defined as

$$n_{vf} = \frac{L_{Bl} * N_{tl}}{L_{LL}} \tag{2.13}$$

where L_{Bl}, N_{tl}, and L_{LL} are the bridge span length, number of span traffic lanes, and overall vehicle length, respectively. The bridge characteristic value n_{vf} shows how many LL trucks can be fully parked on the bridge span to cover all bridge lanes. Secondly, the system RF is defined by combining Equations (2.1) and (2.12) as follows:

$$RF = \frac{(\varphi_c \varphi_s \varphi) * W_{cr}}{(\gamma_{LL}) W_{LL}(1+IM)} \tag{2.14}$$

Equation (2.1) was refined into Equation (2.14) and expressed in terms of unfactored critical weight W_{cr} and LL weight W_{LL}. Now, three possibilities based on estimated RF and n_{vf} values are expected, and an appropriate protocol is proposed for each possibility.

The first protocol is when ($RF \geq n_{vf}$), meaning that bridge span capacity/strength is more than the imposed factored LL trucks even when it is fully loaded by LL. The estimated RF can be declared instantly, and the bridge model is over-designed and can handle more than its

ultimate demand. The second protocol is when ($RF \leq 1$), meaning that the bridge cannot bear even one LL truck on it. In this case, the appropriate action could be issuing a permit LL, legal LL, bridge posting, or bridge replacement plan. The third protocol is when $\left(1 < RF < n_{vf}\right)$, which means the bridge model can handle at least one factored LL but cannot be fully occupied by LL trucks. To be conservative during RF estimation, it is necessary to consider the worst-case scenario to evaluate LL effects on the bridge model. Since BLCP exploits UDL as a simplified loading pattern, an iterative analysis to find the critical LL configuration must be done to enhance RF precision before declaring the simplified RF. Accordingly, a number of LL must be statistically inserted at the bridge FEM to simulate potential worst-case scenario(s) (Hasançebi & Dumlupınar, 2013). A potential worst-case scenario is dictated from the bridge potential failure mode found in the BLCP's fourth stage. The LL configuration produces maximum stress/strain under flexural behavior when the LL is arranged from the middle span toward the sides, regardless of the number of trucks (Albraheemi et al., 2019). Conversely, for bridges with the shear failure mode characteristic, the critical LL configuration is when LL is incrementally imported on the FEM from the model side toward the middle of the span to simulate the worst case (Schanck & Davids, 2020). Depending on the bridge's potential failure mode, the LL is loaded in FEM from 1 to n_{vf} to estimate genuine RF. The same stopping criteria and SLS constraints are valid during this process. Additional help for detecting critical static load configurations is available in the literature (Hernandez & Myers, 2018; Lantsoght, 2019).

Chapter 3 Results

3.1 Finite element model of the benchmark bridge

In order to compare BLCP results with conventional bridge loading capacity evaluation, a sample bridge with well-documented experimental data was chosen for analysis (Sanayei et al., 2012). The Powder Mill Pond Bridge (PMPB) is located in Barre, Massachusetts, as shown in Figure 3.1(a). The PMPB is a three-span continuous composite steel-girder bridge with an RC deck. The bridge is 47 m long with a 23.5 m center span and two 11.75 m outer spans. There are six main girders that run the length of the bridge, evenly spaced at 2.25 m, giving a deck overhang of 732.5 mm.

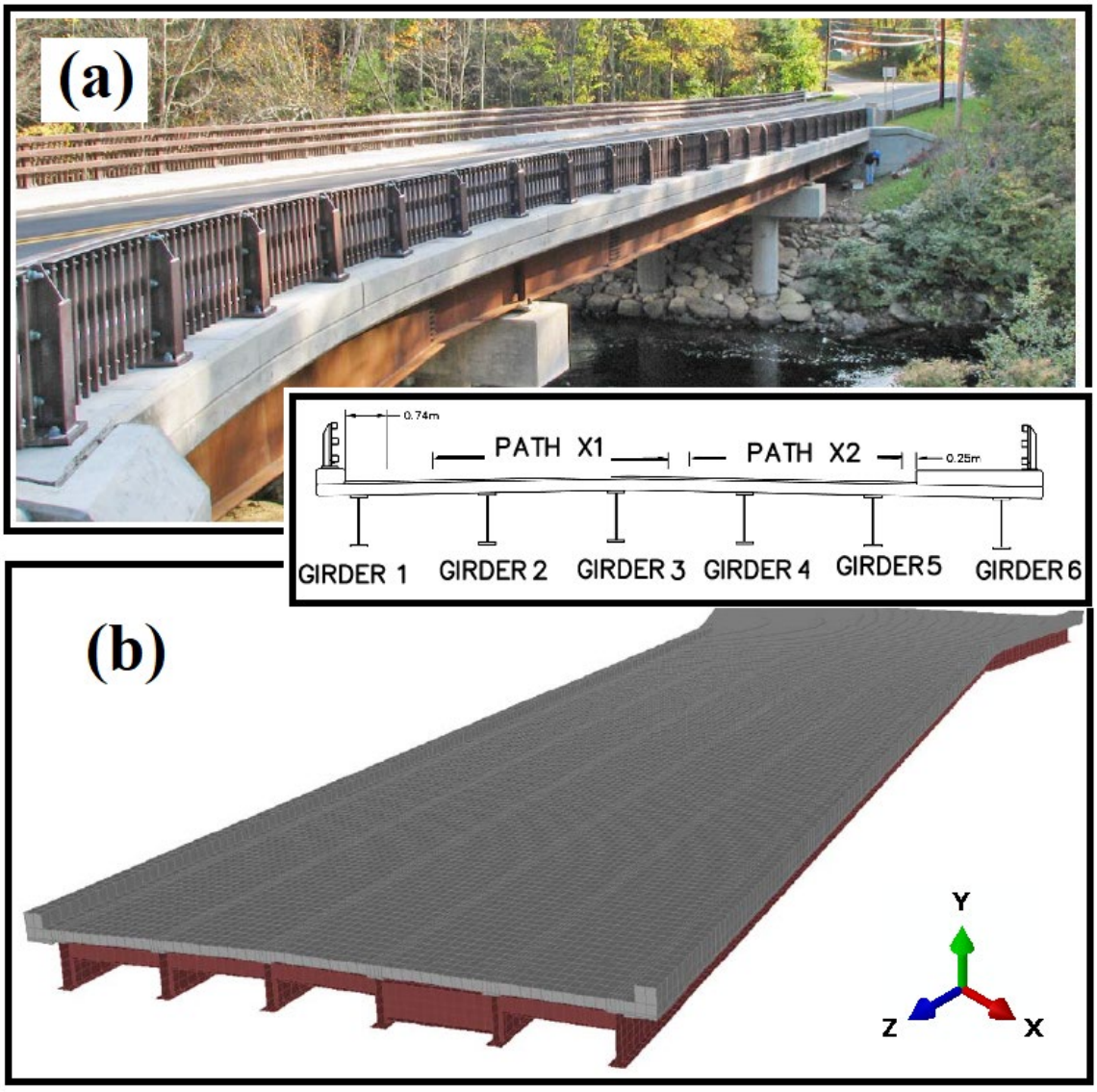

Figure 3.1 The PMPB bridge model; (a) bridge prototype in Massachusetts, courtesy of Sanayei et al. (2012); (b) FEM of the PMPB simulated in Abaqus.

Abaqus® was used to simulate the FEM of the bridge prototype to perform nonlinear static BLCP and dynamic analysis to estimate IM (Dassault Systems Simulia Corp., 2014). The concrete body was modeled with a 3D 8-node isoperimetric element (C3D8R) capable of modeling plastic deformation. The reinforcement rebars were modeled as a 3D wire truss element member (T3D2) plus embedded-region constraints inside the concrete medium. The

embedded-region constraint can satisfy a perfect bond between concrete medium and reinforcement members to accurately simulate a unified reinforcement concrete object. The steel cross beams and girders were modeled with eight nodal points, six degrees of freedom, and a reduced integration shell element (S8R). The self-weight of each bridge part was considered automatically by the software from the material density and part volume. Full composite action between various bridge components was imposed with appropriate FEM constraints. The PMPB FEM is shown in Figure 3.1(b).

3.2 Material models of benchmark FEM

As mentioned previously, BLCP needs all types of nonlinearities to be considered during the process in order to accurately perform bridge loading capacity evaluation and RF estimation. Abaqus has three built-in approaches to modeling concrete damage: the concrete smeared cracking model, the brittle cracking model, and the concrete damage plasticity (CDP) model. The plot of the concrete stress-strain relationship with strengths ranging from 20 MPa to 50 MPa is shown in Figure 3.2(a). The steel material stress-strain behavior was modeled by the nonlinear curve based on Rasmussen's proposed relationship, which is superior to the conventional Ramberg-Osgood model (Rasmussen, 2003). It is an elastic-plastic model with strain hardening in which behavior for both compression and tension is identical. The Abaqus plastic material model was chosen for steel members, assigned by the true stress-strain values. Two steel alloys, steel-37 (ST37) and steel grade-60, were used during FEM coding, and their characteristics were chosen from standards (Carreño et al., 2020). The ST37 was assigned to bridge girders as well as model stringers (cross beams), and steel Grade 60 was assigned to reinforcement and rebars, as shown in Figure 3.2(b).

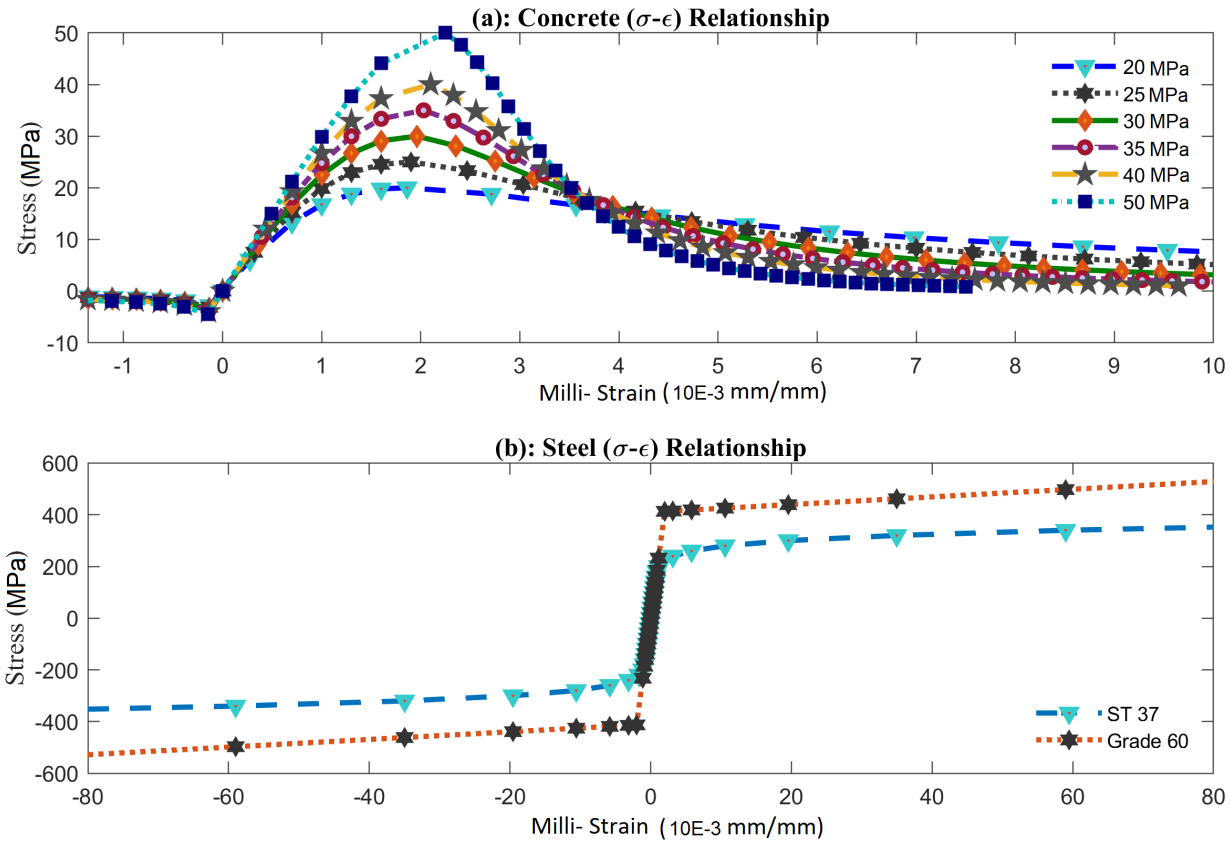

Figure 3.2 Material models: (a) uniaxial behavior stress-strain curves of concrete models; (b) uniaxial stress-strain relationship for structural Steel-37 and Steel Grade-60.

3.3 BLCP results and analysis

After constructing the bridge FEM based on blueprints and material models, both traffic lanes and their affected nodes under AASHTO design load (HL-93 truck) characteristics were defined. Also, the bridge FEM was segmented into several element sets, each at a specific bridge station, in order to capture the first PS as described in the fourth stage of BLCP. The baseline FEM has concrete strength of 30 MPa. A comparison of RFs estimated by traditional AASHTO beam-line analysis, experimental nondestructive testing (NDT) data, and BLCP RFs is plotted in Figure 3.3. It is clear that the BLCP returns unique RF with equal higher values for all girders. The reason it returns better values than other methods is that BLCP can consider the reserve

capacity of the structures, similar to most FEM-based methods. Also, the AASHTO approach is conservative, as reported by other scholars.

Figure 3.3 Rating factor comparison of the AASHTO approach with NDT data and the novel BLCP.

3.4 Dynamic load allowance estimation from FEM

The IM value can be estimated through numerical simulation to be compared with the suggested AASHTO values. Equation (2.6) in the second stage was used to calculate IM values based on various structural responses. The IM indicates how much inertia could escalate the bridge model responses due to truck-induced vibrations. To get an engineering sense of the AASHTO IM value (0.11~0.33) expressed by Equation (2.7), a parametric study was done based on various truck speeds to quantify and compare the FEM IM values with AASHTO values. The Abaqus VDLOAD user subroutine was written in FORTRAN to model moving truck paths with different speeds. The effective nodal sets were selected on the centerlines of each bridge lane,

mimicking the most probable field traffic loadings. This subroutine defines the distributed load magnitude as a function of position, time, and velocity and has been successfully employed by other scholars (Islam et al., 2015).

While the structural responses in Equation (2.6) are commonly inserted based on deflection and stress/strain magnitude values, in this study the IMs were estimated from five different quantities. All deflection, acceleration, angular velocity, concrete maximum principal stress, and total reaction force (TRF) quantities were considered as structural responses in Equation (2.6) to better capture the dynamic traffic loading effects on strength. TRF is equal to the integrated vertical weight that can be computed similar to Equation (2.10), as BLCP imposes incremental loads on traffic lanes. To do so, a parametric study was done in which an HL-93 truck crossed a bridge in its traffic lane with speeds of 16 km/h (10 mph) to 96 km/h (60 mph). The quasi-static response of the bridge can be obtained at a low speed between 5-16 km/h; at this crawling speed, none of the structural modes will be excited (Hernandez & Myers, 2017). To accurately estimate IM during traffic loading, the effective FEM nodes that represent the truck tire contact patch area are selected as two node sets and then dynamically loaded by VDLOAD.

Figures 3.4(a) through 3.4(f) show the raw structural responses of the bridge FEM at their critical spots, and Figure 3.5 shows the corresponding IM values under different truck speeds. The critical spot for displacement, acceleration, and maximum principal stress is in the concrete deck at the midspan, while for angular velocity, it is at the side-span around the bearing system. As explained in the second stage of BLCP, the IM value is prescribed based on road surface condition. On the other hand, the FEM simulation in this study modeled only a very fine road surface condition. Using displacement, stress, and TRF values of the bridge FEM return IM values of about 0.112, which is very close to the AASHTO guideline value ($IM = 0.11$).

Therefore, FEM confirms the AASHTO IM values, at least for the very good road surface condition. Though it is not common to consider acceleration and angular velocity for IM extraction, their effects with a high-speed heavy truck could tremendously affect BLCP. Using structural dynamic responses from very low-speed to high-speed simulation returns IM values to 4.82. This is most likely due to the contribution of higher modes, but since their modal participation factors are low, they have small effects on the structural force and displacement responses (Brandt, 2011).

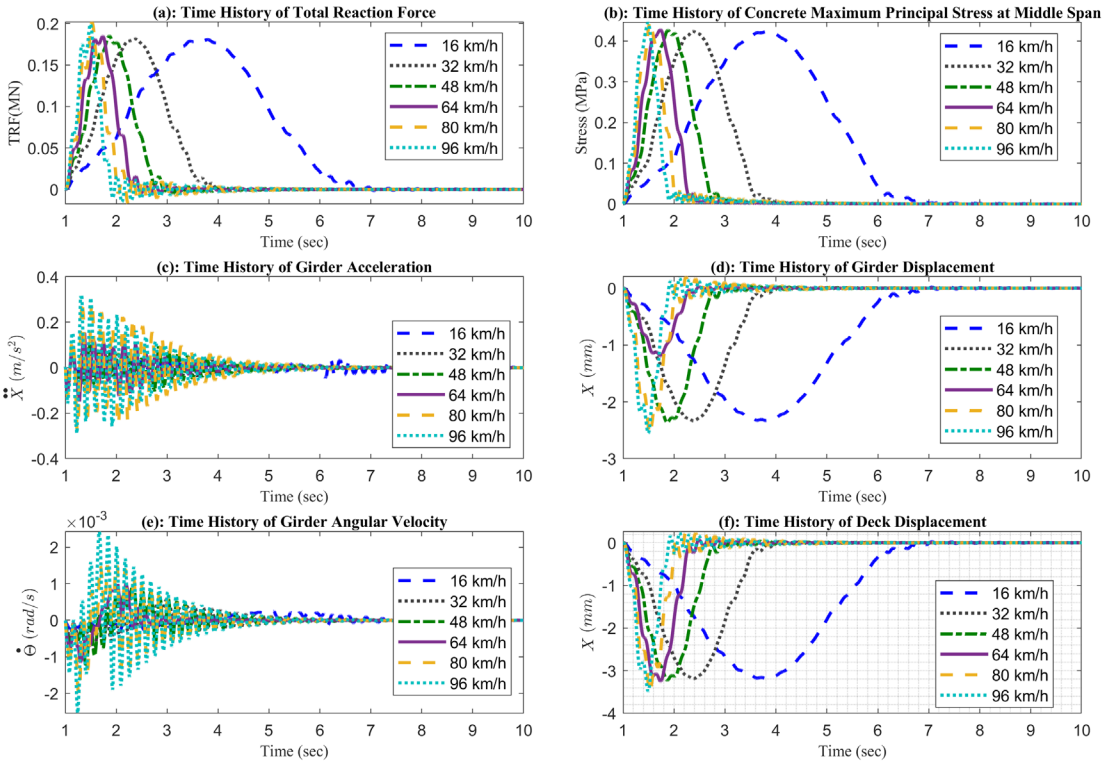

Figure 3.4 FEM dynamic analysis responses: (a) total reaction force; (b) mean value of maximum principal stress in concrete deck at the midspan; (c) girder acceleration at midspan; (d) girder displacement at side-span; (e) girder angular velocity at midspan; (f) deck displacement at midspan.

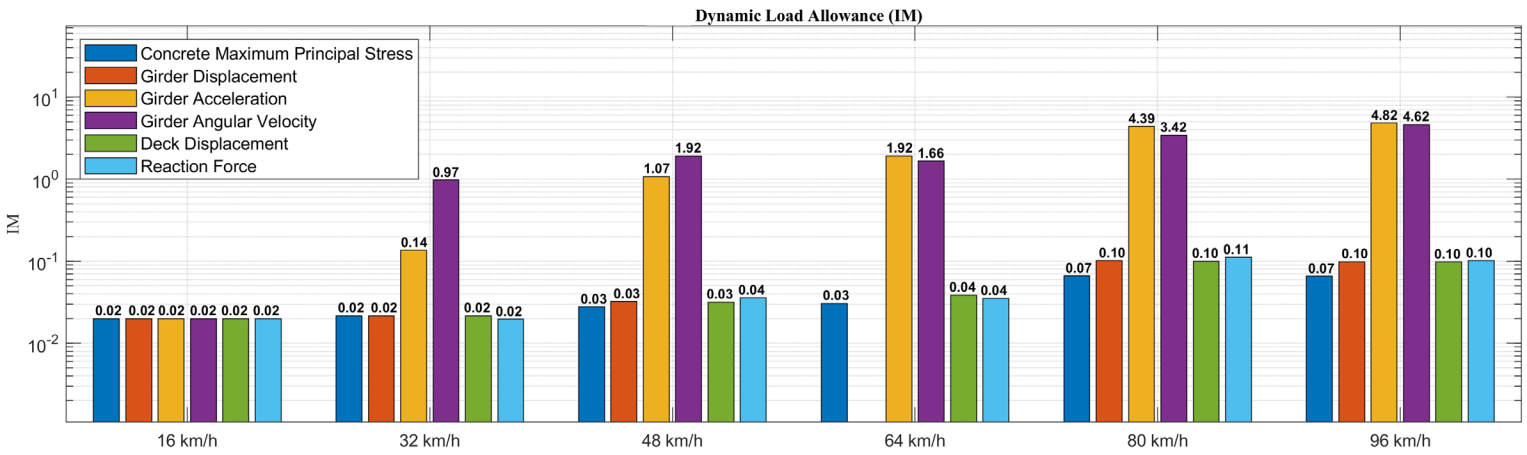

Figure 3.5 Dynamic load allowance (IM) numerically estimated from various structural responses.

Chapter 4 Conclusions

This report proposes a methodology to estimate a bridge's ultimate capacity as well as a unique RF under excessive traffic loading. With the analogy of pushover analysis in seismic engineering, the proposed BLCP philosophy uses a similar concept to impose incremental loading on the traffic lanes to estimate genuine bridge failure mode, ultimate capacity, and associated RF. This unified RF may help DOT authorities to swiftly comprehend overall bridge strength and consequently permit or prohibit specific truck(s) from crossing the bridge. Furthermore, the BLCP algorithm can be appended to the concurrent commercial software to assess bridge integrity by providing a unique RF. This weight-based RF proposed by BLCP is superior to the common methods since it automatically considers combined axial forces, shear forces, and compression/tension moments by using equivalent stress concepts and suitable failure criteria at all 3D FEM segments. So, there is no need to rate individual transformed composite T-beams independently based on AASHTO's strip-width method. Bridge failure mode in case of excessive traffic loading is also identified through BLCP and can be used for the rehabilitation plan depending on the type of failure.

Most of the BLCP formulas and philosophies explained in the third, fourth, and fifth stages are proposed here for the first time to produce a unique RF estimation. In the third stage, the UDL pattern on the traffic lanes was suggested to perform nonlinear finite element analysis to estimate the ultimate bearable weight. With UDL, the weight increases incrementally on the tire contact patch area until one or several PS are initiated and make the bridge model unstable, depending on the structural redundancy. In the fourth stage, the first FEM is segmented equally along the bridge span with consistent element sizes; each segment consists of various elements of different material types for which apt failure criteria have been assigned. Secondly, the concept

of a PS, rather than the common plastic hinge concept in pushover analysis, was defined to capture failure in the 3D domain at critical segment(s) to identify the first PS spot and the corresponding ultimate weight. While common sectional analysis uses the demand and capacity of an equivalent T-beam section to compute overall yielding/PS capacity, BLCP does that process in the 3D domain by deploying appropriate failure criteria depending on the material types in FEM. Thus, there is no need to manually find RF in the negative and positive sections individually since BLCP uses nonlinear FEM to automatically detect failure at the PS when failure criteria were met for all elements of a specific section(s).

All BLCP steps were numerically executed on the PMPB bridge prototype FEM to verify the proposed process and compare it to the well-documented experimental results. Similar to the other FEM-based methods, more capacity was evaluated by BLCP, mostly due to considering whole-system composite actions. As shown in Figure 3.3, the unique BLCP RF is larger than the individual girder RFs estimated by the AASHTO approach as well as NDT data. The AASHTO results are conservative about BLCP due to the high-reliability distribution factors, as repeatedly reported by other scholars. The bridge dynamic responses and nonlinear static force-displacement responses indicate realistic bridge behaviors under extreme traffic. The increase of force after the yielding point in the curves is due to the hardening of the material after yielding. This causes the realistic bridge capacity to increase after the first PS initiates, based on LRFD code.

Finally, another interesting finding was the IM value for the benchmark bridge compared to the AASHTO guideline. Although road roughness was not incorporated in this study, the FEM IM value was very close to the AASHTO value for the clean road surface condition in terms of displacement, TRF, and stress quantities, though the IM value estimation needs advanced

numerical simulation for poor road surface condition and modeling bumps. Although acceleration and angular velocity responses have not yet been used for IM estimation, this study shows they attain high values even for a very good road surface condition. Their high values mostly come from higher structural mode contributions, and it is strongly suggested their fatigue and secondary dynamic effects be further studied.

References

Aghagholizadeh, M., & Catbas, N. (2019). Comparative analysis and evaluation of two prestressed girder bridges. Current Trends in Civil & Structural Engineering, 3(5). http://dx.doi.org/10.33552/CTCSE.2019.03.000572

Albraheemi, M. J. A., Davids, W. G., Schanck, A., & Tomlinson, S. (2019). Evaluation and rating of older non-composite steel girder bridges using field live load testing and nonlinear finite element analysis. Bridge Structures, 15(1-2), 27–41. https://doi.org/10.3233/BRS-190150

Alinia, M. M., Shakiba, M., & Habashi, H. R. (2009). Shear failure characteristics of steel plate girders. Thin-Walled Structures, 47(12), 1498–1506. https://doi.org/10.1016/j.tws.2009.06.002

American Association of State Highway Transportation Officials. (2017). LRFD bridge design specifications (8th ed.).

American Association of State Highway Transportation Officials. (2018). Manual for bridge evaluation (3rd ed.).

American Association of State Highway Transportation Officials. (2020). AASHTOWare: Bridge analysis and rating software. https://www.aashtoware.org

Bakht, B., & Mufti, A. (2015). Bridges: Analysis, design, structural health monitoring, and rehabilitation. Springer International Publishing AG.

Benčat, J., & Kohár, R. (2018). Bridges subjected to dynamic loading. In H. Yaghoubi (Ed.), Bridge engineering (p. 111). http://dx.doi.org/10.5772/intechopen.73193

Brandt, A. (2011). Noise and vibration analysis: signal analysis and experimental procedures. Wiley.

Cao, R., Agrawal, A. K., El-Tawil, S., Xu, X., & Wong, W. (2019). Performance-based design framework for bridge piers subjected to truck collision. Journal of Bridge Engineering, 24(7), 04019064. https://doi.org/10.1061/(ASCE)BE.1943-5592.0001423

Carreño, R., Lotfizadeh, K. H., Conte, J. P., & Restrepo, J. I. (2020). Material model parameters for the Giuffrè-Menegotto-Pinto uniaxial steel stress-strain model. Journal of Structural Engineering, 146(2), 04019205. https://doi.org/10.1061/(ASCE)ST.1943-541X.0002505

Dassault Systems Simulia Corp. (2014). Abaqus theory guide. In Abaqus 6.14. http://ivt-abaqusdoc.ivt.ntnu.no:2080/v6.14/books/stm/default.htm

Deng, L., & Cai, C. S. (2010). Development of dynamic impact factor for performance evaluation of existing multi-girder concrete bridges. Engineering Structures, 32(1), 21–31. https://doi.org/10.1016/j.engstruct.2009.08.013

Deng, L., Cai, C. S., & Barbato, M. (2011). Reliability-based dynamic load allowance for capacity rating of prestressed concrete girder bridges. Journal of Bridge Engineering, 16(6), 872–880. https://doi.org/10.1061/(ASCE)BE.1943-5592.0000178

Deng, Y., & Phares, B. M. (2016). Automated bridge load rating determination utilizing strain response due to ambient traffic trucks. Engineering Structures, 117, 101–117. https://doi.org/10.1016/j.engstruct.2016.03.004

Dymond, B. Z., French, C. E., & Shield, C. K. (2019). Recommendations for more accurate shear rating of prestressed concrete girder bridges. Journal of Bridge Engineering, 24(12), 04019117. https://doi.org/10.1061/(ASCE)BE.1943-5592.0001495

Garcia, M. S. C., Siqueira, G. H., Viera Junior, L. C. M., & Vizotto, I. (2019). Evaluation of structural capacity of triangular and hexagonal reinforced concrete free-form

shells. Engineering Structures, 188, 519–537. https://doi.org/10.1016/j.engstruct.2019.03.044

Hasançebi, O., & Dumlupınar, T. (2013). Detailed load rating analyses of bridge populations using nonlinear finite element models and artificial neural networks. Computers & Structures, 128, 48–63. https://doi.org/10.1016/j.compstruc.2013.08.001

Hernandez, E. S., & Myers, J. J. (2017). Dynamic load allowance of a prestressed concrete bridge through field load tests. Proceedings of the SMAR 2017 Fourth Conference on Smart Monitoring, Assessment and Rehabilitation of Civil Structures. https://data.smar-conferences.org/SMAR_2017_Proceedings/papers/251.pdf

Hernandez, E. S., & Myers, J. J. (2018). Strength evaluation of prestressed concrete bridges by load testing. Life Cycle Analysis and Assessment in Civil Engineering: Towards an Integrated Vision: Proceedings of the Sixth International Symposium on Life-Cycle Civil Engineering (IALCCE 2018), 5, 169. CRC Press.

Islam, A. A., Jaroo, A. S., & Li, F. (2015). Bridge load rating using dynamic response. Journal of Performance of Constructed Facilities, 29(4), 04014120. https://doi.org/10.1061/(ASCE)CF.1943-5509.0000620

Jamali, S., Chan, T. H., Nguyen, A., & Thambiratnam, D. P. (2019). Reliability-based load-carrying capacity assessment of bridges using structural health monitoring and nonlinear analysis. Structural Health Monitoring, 18(1), 20–34. https://doi.org/10.1177/1475921718808462

Lantsoght, E. O. (Ed.). (2019). Load testing of bridges: Current practice and diagnostic load testing. CRC Press.

Leckie, F. A., & Bello, D. J. D. (Eds). (2009). Failure criteria. In Strength and stiffness of engineering systems. Springer. https://doi.org/10.1007/978-0-387-49474-6_9

Lee, J. J., Cho, S., Shinozuka, M., Yun, C. B., Lee, C. G., & Lee, W. T. (2006). Evaluation of bridge load carrying capacity based on dynamic displacement measurement using real-time image processing techniques. International Journal of Steel Structures, 6(5), 377–385.

Liu, Y., Kuang, J. S., & Yuen, T. Y. (2020). Modal-based ground motion selection procedure for nonlinear response time history analysis of high-rise buildings. Earthquake Engineering and Structural Dynamics, 49(1), 95–110. https://doi.org/10.1002/eqe.3232

Peng, C., El Damatty, A. A., Musa, A., & Hamada, A. (2020). Simplified numerical approach for the lateral load analysis of light-frame wood shear wall structures. Engineering Structures, 219, 110921. https://doi.org/10.1016/j.engstruct.2020.110921

Rasmussen, K. J. (2003). Full-range stress-strain curves for stainless steel alloys. Journal of Constructional Steel Research, 59(1), 47–61. https://doi.org/10.1016/S0143-974X(02)00018-4

Rosendahl, P. L., Drass, M., Felger, J., Schneider, J., & Becker, W. (2019). Equivalent strain failure criterion for multiaxially loaded incompressible hyperelastic elastomers. International Journal of Solids and Structures, 166, 32–46. https://doi.org/10.1016/j.ijsolstr.2019.01.030

Russian, O., Belarbi, A., Feng, Q., & Dawood, M. (2020). Investigation of material properties for load rating of historical bridges. Journal of Bridge Engineering, 25(4), 04020014. https://doi.org/10.1061/(ASCE)BE.1943-5592.0001540

Sanayei, M., Phelps, J.E., Sipple, J.D., Bell, E.S. and Brenner, B.R., 2012. Instrumentation, nondestructive testing, and finite-element model updating for bridge evaluation using

strain measurements. Journal of bridge engineering, 17(1), pp.130-138. https://doi.org/10.1061/(ASCE)BE.1943-5592.0000228

Schanck, A. P., & Davids, W. G. (2020). Capacity assessment of older t-beam bridges by nonlinear proxy finite-element analysis. Structures, 23, 267–278. https://doi.org/10.1016/j.istruc.2019.09.012

Shahsavari, V., Mehrkash, M., & Santini-Bell, E. (2020). Damage detection and decreased load-carrying capacity assessment of a vertical-lift steel truss bridge. Journal of Performance of Constructed Facilities, 34(2), 04019123. https://doi.org/10.1061/(ASCE)CF.1943-5509.0001400

Siavashi, S., & Eamon, C. D. (2019). Development of traffic live-load models for bridge superstructure rating with RBDO and best selection approach. Journal of Bridge Engineering, 24(8), 04019084. https://doi.org/10.1061/(ASCE)BE.1943-5592.0001457

Tian, Y., & Zhang, J. (2020). Structural flexibility identification via moving-vehicle-induced time-varying modal parameters. Journal of Sound and Vibration, 474, p. 115264. https://doi.org/10.1016/j.jsv.2020.115264

Tohme, R., & Yarnold, M. (2020). Steel bridge load rating impacts owing to autonomous truck platoons. Transportation Research Record, 2674(2), 57–67. https://doi.org/10.1177/0361198120902435

Varela-Ortiz, W., Cintrón, C. Y. L., Velázquez, G. I., & Stanton, T. R. (2013). Load testing and GPR assessment for concrete bridges on military installations. Construction and Building Materials, 38, 1255–1269. https://doi.org/10.1016/j.conbuildmat.2010.09.044

Vu, Q. V., Thai, D. K., & Kim, S. E. (2018). Effect of intermediate diaphragms on the load–carrying capacity of steel–concrete composite box girder bridges. Thin-Walled Structures, 122, 230–241. https://doi.org/10.1016/j.tws.2017.10.024

Xu, X., Cao, R., El-Tawil, S., Agrawal, A. K., & Wong, W. (2019). Loading definition and design of bridge piers impacted by medium-weight trucks. Journal of Bridge Engineering, 24(6), p.04019042. https://doi.org/10.1061/(ASCE)BE.1943-5592.0001397